Simulation Study of ECCD in Helical Plasmas*)

Yohei MORIYA, Sadayoshi MURAKAMI and Kazunobu NAGASAKI[1)]

Department of Nuclear Engineering, Kyoto University, Kyoto 606-8501, Japan
[1)]*Institute of Advanced Energy, Kyoto University, Uji 611-0011, Japan*

(Received 19 January 2011 / Accepted 28 July 2011)

The electron cyclotron current drive (ECCD) is studied in Heliotron J and LHD plasmas using GNET code in order to study the ECCD physics in helical configurations. The magnetic configuration dependence of ECCD is investigated in the Heliotron J plasma. It is found that the current direction is reversed in high bumpiness configuration compared with the other configurations. The ECCD in LHD is also investigated by changing electron cyclotron heating points fixing the configuration. It is found that the direction of the current reverses when we change the heating point from the ripple top to the ripple bottom.

Keywords: ECH, ECCD, helical system, Heliotron J, LHD, Fisch-Boozer effect, Ohkawa effect

DOI: 10.1585/pfr.6.2403139

1. Introduction

Electron Cyclotron Current Drive (ECCD) is one of the reliable methods to drive a plasma current by injecting the electron cyclotron wave. The electron cyclotron wave has the GHz range of frequency and the wave absorption position can be controlled locally by changing the magnetic field strength. Consequently, ECCD can control current profile locally and has been applied for toroidal devices to keep the current profile, to stabilize MHD instabilities and to cancel the bootstrap current in helical systems.

There are two well known ECCD mechanisms, namely the Fisch-Boozer effect and the Ohkawa effect [1, 2]. These effects drive the current of opposite directions. The Fisch-Boozer effect assumes the case where the perpendicular velocity direction shift of electrons with finite positive $v_{\parallel}$ is caused by ECH in velocity space. Asymmetry is generated by this shift in velocity space and it relaxes to Maxwell distribution through the collisional process. Here, collision frequency of energetic electron decreases in proportional to v^{-3}, where v is the electron velocity. So the collisional relaxation of high energy electrons is slower than that of low energy electrons. This difference of the relaxation time causes an excess of electrons moving with positive $v_{\parallel}$. Therefore the negative toroidal current is driven by ECH. This current drive mechanism is called the Fisch-Boozer effect.

The Ohkawa effect occurs in a toroidal configuration, where a trapped particle exists by the toroidal mirror field. If the electrons accelerated by ECH are shifted from the passing particle region to the trapped particle region, the asymmetry in the $v_{\parallel}$ direction of these electrons is lost rapidly because of the bounce motion of the trapped electrons. The bounce motion symmetrizes the distribution in velocity space more rapidly than the collisional ones and the asymmetry due to the deficit of electrons in the low energy region remains. So the excess of electron deficit with $v_{\parallel}$ drives the positive toroidal current. This mechanism is called the Ohkawa effect.

In order to study the ECCD physics, a number of ECCD experiments have been performed in many devices [3]. Especially in Heliotron J, which is the helical-axis heliotron device, EC currents were measured experimentally and ECCD dependence on the magnetic configuration and the density were obtained [4, 5]. It was found that the EC current decreased as electron density was increased and that the current changed depending on magnetic configurations. Moreover, it was observed that the direction of the EC current was reversed in high bumpiness configuration compared with the other magnetic configurations. In LHD, in order to investigate the characteristics of EC driven current and to make clear the possibility of controlling the current and rotational transform profiles, ECCD experiments have been performed [6].

While the experimental analyses of ECCD have been carried out in the number of helical devices as mentioned above, the theoretical analyses of these experiments have not been done sufficiently. In this study, we simulate the current drive on helical plasmas by GNET code in order to make clear the ECCD physics. GNET has been developed for transport study of high energy electrons in helical systems, and has been applied to ECCD analysis in helical systems. The objective of this study is to make it clear the effect of trapped electrons on ECCD. The EC driven currents are evaluated changing the magnetic configuration and the heating points in Heliotron J and LHD.

author's e-mail: moriya@p-grp.nucleng.kyoto-u.ac.jp

*) This article is based on the presentation at the 20th International Toki Conference (ITC20).

2. Simulation Model

GNET code can solve the linearized drift kinetic equation as a (time-dependent) initial value problem based on the Monte Carlo technique (in 5-D phase space) [7]. A technique similar to the adjoint equation for dynamic linearized problems is used and the linearized drift kinetic equation for the deviation from the Maxwellian background, δf, is solved. We can obtain the steady state solution of the distribution function by GNET. In helical system the motion of trapped particles becomes complicated because of the complex 3-D magnetic configuration. Therefore, in order to analyze ECH in detail on helical systems, we have to take account of the radial diffusion of trapped particles. And, to do so, we must consider the distribution function at least in 5-D phase space. We can analyze ECCD in detail on complex helical configurations by GNET.

In GNET the gyrophase averaged electron distribution function is described as

$$f(\boldsymbol{x}, v_\parallel, v_\perp, t) = f_{\rm Max}(r, v^2) + \delta f(\boldsymbol{x}, v_\parallel, v_\perp, t), \tag{1}$$

where $f_{\rm Max}(r, v^2)$ represents a Maxwellian depending on the effective radius r. The linearized drift kinetic equation can be written with the initial condition $\delta f(\boldsymbol{x}, v_\parallel, v_\perp, t = 0) = 0$ as

$$\frac{\partial \delta f}{\partial t} + (\boldsymbol{v}_{\rm d} + \boldsymbol{v}_\parallel) \cdot \frac{\partial \delta f}{\partial \boldsymbol{x}} + \dot{\boldsymbol{v}} \cdot \frac{\partial \delta f}{\partial \boldsymbol{v}} = C^{\rm coll}(\delta f) + L^{\rm orbit}(\delta f) + S^{\rm ql}(f_{\rm Max}), \tag{2}$$

where $\boldsymbol{v}_{\rm d}$ is the drift velocity and $\boldsymbol{v}_\parallel (= v_\parallel \hat{\boldsymbol{b}})$ is the parallel velocity. The acceleration term $\dot{\boldsymbol{v}} = \dot{\boldsymbol{v}}_\parallel + \dot{\boldsymbol{v}}_\perp$ is given by the conservation of magnetic moment and total energy. $C^{\rm coll}$ and $L^{\rm orbit}$ are the linearized collision operator and the particle loss term, respectively. $S^{\rm ql}$ represents the quasilinear source term.

It is convenient to introduce the Green's function $\mathcal{G}(\boldsymbol{x}, v_\parallel, v_\perp, t | \boldsymbol{x}', v_\parallel', v_\perp')$, which is defined by the homogeneous Fokker-Planck equation corresponding to Eq. (2), as

$$\frac{\partial \mathcal{G}}{\partial t} + (\boldsymbol{v}_{\rm d} + \boldsymbol{v}_\parallel) \cdot \frac{\partial \mathcal{G}}{\partial \boldsymbol{x}} + \dot{\boldsymbol{v}} \cdot \frac{\partial \mathcal{G}}{\partial \boldsymbol{v}} - C^{\rm coll}(\mathcal{G}) - L^{\rm orbit}(\mathcal{G}) = 0, \tag{3}$$

where the initial condition is $\mathcal{G}(\boldsymbol{x}, \boldsymbol{v}, t = 0 | \boldsymbol{x}', \boldsymbol{v}') = \delta(\boldsymbol{x} - \boldsymbol{x}')\delta(\boldsymbol{v} - \boldsymbol{v}')$. An electron starting at the time $t = 0$ at the position $\boldsymbol{x}'$ with the velocity $\boldsymbol{v}'$ will be found with the probability

$$\mathcal{G}(\boldsymbol{x}, \boldsymbol{v}, t | \boldsymbol{x}', \boldsymbol{v}') {\rm d}\boldsymbol{x} {\rm d}\boldsymbol{v}, \tag{4}$$

at the time t in the phase space volume element ${\rm d}\boldsymbol{x}{\rm d}\boldsymbol{v}$ centered at $\boldsymbol{x}, \boldsymbol{v}$. The solution for δf is given by the convolution of $S^{\rm ql}$ with $\mathcal{G}$,

$$\delta f(\boldsymbol{x}, \boldsymbol{v}, t) = \int_0^t {\rm d}t' \int {\rm d}\boldsymbol{x}' \int {\rm d}\boldsymbol{v}' \times S^{\rm ql}[f_{\rm Max}(r', v'^2)] \mathcal{G}(\boldsymbol{x}, \boldsymbol{v}, t - t' | \boldsymbol{x}', \boldsymbol{v}'). \tag{5}$$

Therefore, if this Green's function is obtained, the solution of Eq. (2) is also derived from Eq. (5) and we can obtain the steady state distribution function of high energy electrons.

We follow the test particle orbits to evaluate the Green function in Boozer coordinates on the bases of a 3D MHD equilibrium. A 6th-order Runge-Kutta-Huta method is applied to integrate the equation of motion using the magnetic field data. The collisional effects (both pitch angle and energy scattering) are taken into account using the linear Monte Carlo collision operator. The particle collision by the s-species (electron and ions) is given by

$$C_s^{\rm coll}(\delta f) = \frac{1}{v^2}\frac{\partial}{\partial v}\left[v^2 \nu_{\rm E}^2 \left(v\delta f + \frac{T_s}{m}\frac{\partial \delta f}{\partial v}\right)\right] + \frac{\nu_{\rm d}^s}{2}\frac{\partial}{\partial \lambda}(1 - \lambda^2)\frac{\partial \delta f}{\partial \lambda}, \tag{6}$$

where $\lambda = v_\parallel / v$, and $\nu_{\rm E}^2$ and $\nu_{\rm d}^s$ are the energy transfer rate and the deflection collision frequency by a background of s-species particles, respectively. The model developed by Boozer and Kuo-Petravic [8] is applied in the simulation evaluating the Green function.

$S^{\rm ql}$ represents the change in velocity space caused by ECH. Because we assume a quasilinear heating term, the multi-interaction with EC waves is not taken into account. Thus the resonant interaction is not considered in solving Eq. (3) that is important in the ICRF heating.

We assume $S^{\rm ql} = S_+ - S_-$, where S_+ (the source term) and S_- (the sink term) are the increase and decrease of the distribution function, respectively. Because ECH shifts the velocity of electrons in the perpendicular direction, we assume S_+ and S_- as

$$S_+ = \frac{S_0}{2\pi v_\perp}\delta(\rho - \rho_0)\delta(\theta - \theta_0)\delta(\phi - \phi_0) \times \delta(v_\parallel - \alpha_\parallel v_{\rm th})\delta(v_\perp - \alpha_+ v_{\rm th}), \tag{7}$$

$$S_- = \frac{S_0}{2\pi v_\perp}\delta(\rho - \rho_0)\delta(\theta - \theta_0)\delta(\phi - \phi_0) \times \delta(v_\parallel - \alpha_\parallel v_{\rm th})\delta(v_\perp - \alpha_- v_{\rm th}), \tag{8}$$

where $\rho = r/a$ is normalized radial position, θ and ϕ correspond to poloidal and toroidal angles, respectively. Subscript 0 of ρ_0, ϕ_0 and θ_0 means a heating position. $v_{\rm th}$ corresponds to thermal velocity of electron, and $\alpha_\parallel v_{\rm th}$ and $\alpha_\pm v_{\rm th}$ are respectively the parallel and perpendicular velocity of the heated electrons. The amplitude S_0 of each terms depends on ECH heating power $P_{\rm ECH}$. Using $E_\pm$, electron energy before and after heating, $P_{\rm ECH}$ is given by

$$\begin{aligned} P_{\rm ECH} &= \int \{S_+(\boldsymbol{x}, \boldsymbol{v})E_+(\boldsymbol{v}) - S_-(\boldsymbol{x}, \boldsymbol{v})E_-(\boldsymbol{v})\}\, {\rm d}\boldsymbol{x}{\rm d}\boldsymbol{v} \\ &= \int \{S_+(\boldsymbol{x}, v_\parallel, v_\perp)E_+(v_\parallel, v_\perp) \\ &\quad - S_-(\boldsymbol{x}, v_\parallel, v_\perp)E_-(v_\parallel, v_\perp)\}\, 2\pi v_\perp {\rm d}\boldsymbol{x}{\rm d}v_\parallel {\rm d}v_\perp \\ &= S_0 E_+(\alpha_\parallel v_{\rm th}, \alpha_+ v_{\rm th}) - S_0 E_-(\alpha_\parallel v_{\rm th}, \alpha_- v_{\rm th}). \end{aligned}$$

$E_\pm$ are described as $E_\pm(\alpha_\parallel v_{\rm th}, \alpha_\pm v_{\rm th}) = E_{\rm th} \cdot (\alpha_\parallel^2 + \alpha_\pm^2)$, where $E_{\rm th}$ is electron energy moving with $v_{\rm th}$. Therefore, $P_{\rm ECH}$ is

denoted as

$$P_{\mathrm{ECH}} = S_0 E_{\mathrm{th}} \cdot (\alpha_+^2 - \alpha_-^2), \tag{9}$$

and so S_0 is given by

$$S_0 = \frac{P_{\mathrm{ECH}}}{E_{\mathrm{th}} \cdot (\alpha_+^2 - \alpha_-^2)}. \tag{10}$$

Eqs. (7) and (8) represent the increase and decrease of distribution function as a δ function. We assume a very simple model as a first step.

3. Simulation Result

3.1 Result of Heliotron J simulation

Various magnetic configurations are capable in Heliotron J device by changing the ratio of coil currents. Here we consider bumpiness ε_b, which is the parameter characterizing magnetic configurations given by

$$\varepsilon_b = B_{04}/B_{00}, \tag{11}$$

where B_{mn} represents the Fourier component of the magnetic field strength in Boozer coordinates, and m and n are the poloidal and toroidal mode numbers, respectively. In this study we assume three configurations, namely ε_b = 0.01 (low bumpiness), ε_b = 0.06 (medium bumpiness) and ε_b = 0.15 (high bumpiness) at ρ = 0.67. The distribution of the magnetic field strength along the magnetic axis in these bumpiness are shown in Fig. 1. From this figure, EC power is deposited at the top of the magnetic ripple in the low bumpiness (ε_b = 0.01). On the other hand, EC power is deposited at the bottom of the ripple in the high bumpiness (ε_b = 0.15). ε_b = 0.06 is the standard magnetic configuration.

We estimate the dependence of EC current on magnetic configurations in the three configurations. We assume the heating point of the source and sink terms as ρ_0 = 0.1, θ_0 = 0° and ϕ_0 = 45° and the heating parameters as $\alpha_{\|}$ = 1.0, α_+ = 2.5, α_- = 1.5 and P_{ECH} = 350 kW

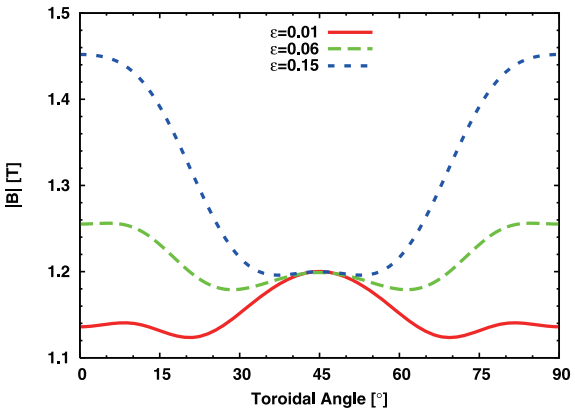

Fig. 1 The distribution of the magnetic field strength along the magnetic axis. EC wave is absorbed at ϕ = 45°.

according to the heating condition on the experiments in Heliotron J. The obtained distribution functions by GNET in the low bumpiness and high bumpiness cases are shown in Fig. 2. The increase and decrease from Maxwellian are colored with red and blue, respectively.

In the low bumpiness case (Fig. 2 (a)), it is considered that ECH accelerated electrons are hardly trapped. The collisional relaxation of the electron deficit in low energy region is faster than that of the accelerated electrons. This results in the excess of electrons with positive $v_{\|}$ and so the negative toroidal current is driven. Consequently, we can see that the current is driven by the Fisch-Boozer effect.

In the high bumpiness case (Fig. 2 (b)), since the EC wave is absorbed at the bottom of the magnetic ripple, many accelerated electrons become trapped electrons. From Fig. 2 (b) it is found that the distribution of the high energy region becomes symmetric rapidly while the distribution of the low energy region becomes symmetric slowly by the collisional relaxation. As a result, the excess of low energy electron deficit with $v_{\|}$ is caused by ECH. Therefore it is found that the positive toroidal current is driven by the Ohkawa effect.

EC current can be calculated by integrating the distribution function on velocity space. We estimate the EC current in three configuration cases. The obtained EC current are summarized in Fig. 3. It is found that the negative currents are driven in ε_b = 0.01 and ε_b = 0.06, on the other hand, the positive current is driven in ε_b = 0.15. So the current direction is reversed between the high bumpiness and the other configuration cases. I_+, the current driven by

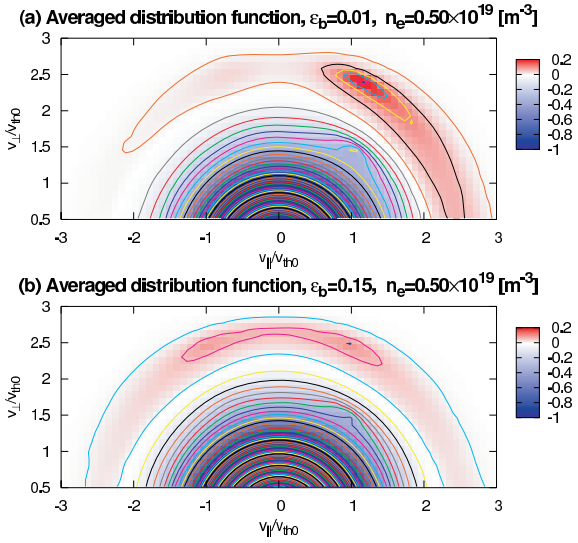

Fig. 2 The results in Heliotron J simulations. Flux averaged distribution functions of (a) ε_b = 0.01 and (b) ε_b = 0.15 are plotted in velocity space. The increase (δf_+) and decrease (δf_-) from Maxwellian are colored with red and blue, respectively. These results are calculated in $n_e = 0.50 \times 10^{19}$ m^{-3}, T_e = 1 keV, where n_e is electron density and T_e is electron temperature.

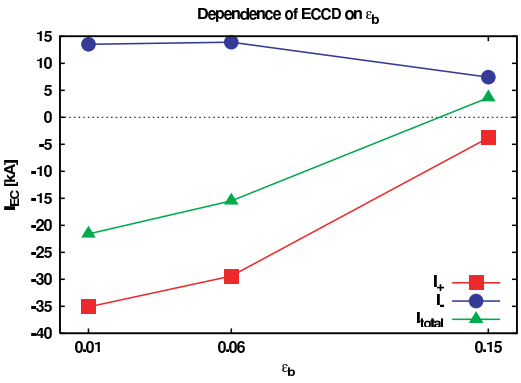

Fig. 3 The ECCD dependence on magnetic configurations in Heliotron J. The simulation results on three configurations are plotted. $I_{\rm total}$ is calculated from total distribution function. I_+ and I_- are calculated from δf_+ and δf_-. These current values are the results in $n_{\rm e} = 0.50 \times 10^{19}$ m^{-3}, $T_{\rm e} = 1$ keV.

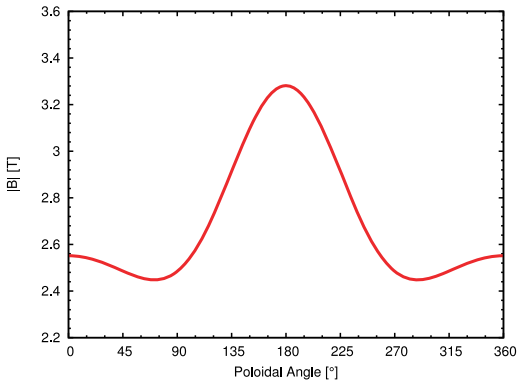

Fig. 4 The dependence of the magnetic field strength on the poloidal angle θ. ρ and ϕ are fixed 0.6 and 0°.

the excess of high energy electrons with $+v_\parallel$ becomes large in the low and medium bunmpiness. In the high bumpiness case, by contrast, asymmetry of high energy electron is lost due to bounce motion and I_+ becomes nearly zero. Therefore the remaining deficit of low energy electrons mainly contributes to current drive. So the current is driven mainly by the Fisch-Boozer effect in $\varepsilon_{\rm b} = 0.01$ and $\varepsilon_{\rm b} = 0.06$ configurations. On the other hand, the Ohkawa effect exceeds the Fisch-Boozer effect and so the current direction reverses in $\varepsilon_{\rm b} = 0.15$ configuration. The obtained magnetic configuration dependences by GNET simulations qualitatively agree with the experimental ones.

3.2 Result of LHD simulation

In the LHD case, we estimate the EC current changing the ECH heating points. The variation of the magnetic field strength along the toroidal and poloidal directions becomes large on flux surface $\rho \sim 0.6$ in the LHD configuration. Here, the magnetic field strength along the poloidal angle θ at the toroidal angle $\phi = 0°$ (vertically elongated cross section) is shown in Fig. 4. We expect that when the EC wave is absorbed at $\theta_0 = 90°$ or the ripple bottom, many trapped electrons are generated, but in the case where the EC power is deposited at $\theta_0 = 180°$ or the ripple top, accelerated electrons are scarcely trapped. Based on this expectation, we simulate ECCD by changing θ_0 from 0° to 180°, assuming EC wave is absorbed at $(\rho_0, \phi_0) = (0.6, 0°)$. The other parameters of the source and sink terms are assumed as $\alpha_\parallel = 1.0$, $\alpha_+ = 2.5$, $\alpha_- = 1.5$ and $P_{\rm ECH} = 1000$ kW.

Figure 5 shows the simulation results of three heating points. In the case of $(\rho_0, \phi_0, \theta_0) = (0.6, 0°, 0°)$ and $(0.6, 0°, 90°)$ (Fig. 5 (a), (b)), the asymmetry in the high energy region is lost due to the effect of the bounce motion. Consequently, the positive toroidal current is driven by the asymmetry in the low energy electrons. On the other hand, trapped electrons are scarcely generated in the

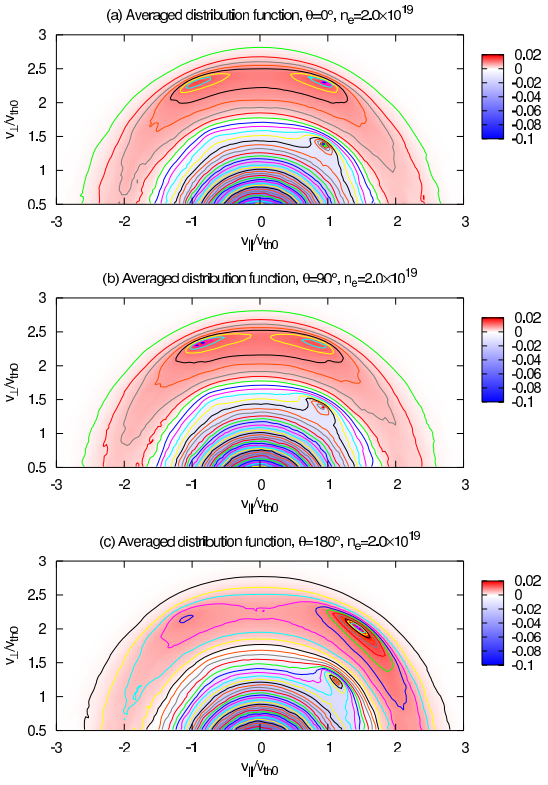

Fig. 5 The results in LHD simulations. Flux averaged distribution function of (a) $\theta_0 = 0°$, (b) $\theta_0 = 90°$ and (c) $\theta_0 = 180°$ are plotted in velocity space. The increase (δf_+) and decrease (δf_-) from Maxwellian are colored with red and blue, respectively. These results are calculated in $n_{\rm e} = 2.0 \times 10^{19}$ m^{-3}, $T_{\rm e} = 1.5$ keV.

case of $(\rho_0, \phi_0, \theta_0) = (0.6, 0°, 180°)$ (Fig. 5 (c)). Thus the $v_\parallel$ asymmetry in the high energy region remains and the negative toroidal current is driven.

We evaluated the EC current from the distribution functions and investigated the ECCD dependence on ECH heating points. This dependence is summarized in Fig. 6. It is found that the current is driven mainly by the Fisch-Boozer effect in the ripple top heating case ($135° < \theta_0 < 180°$), while the Ohkawa effect exceeds the Fisch-Boozer

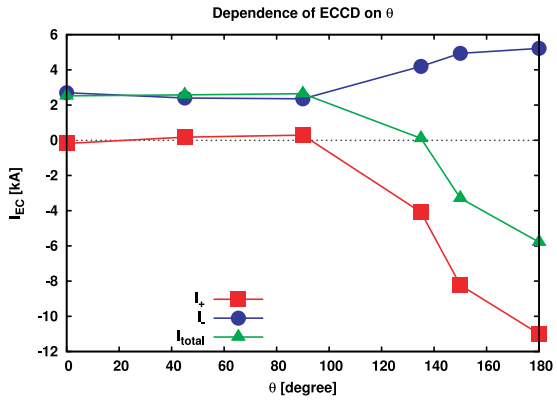

Fig. 6 The ECCD dependence on ECH heating points. These results are calculated in $n_e = 2.0\times10^{19}$ m^{-3}, $T_e = 1.5$ keV. I_{total} is calculated from total distribution function. I_+ and I_- are calculated from δf_+ and δf_-.

effect in the ripple bottom heating case ($0° < \theta_0 < 135°$).

4. Conclusion

In order to study the ECCD physics on helical plasmas, we have simulated the current drive of ECH plasmas in Heliotron J and LHD by GNET. In the Heliotron J case, we have analyzed ECCD assuming three magnetic configurations similar to the experimental ones. Simulation results have shown that the direction of EC current was reversed in the high bumpiness configuration compared with the low and medium bumpiness configurations. We found that EC current changed depending on magnetic configurations and obtained current direction was determined by the balance between the Fisch-Boozer effect and the Ohkawa effect. In the LHD case, we have simulated ECCD by changing ECH heating points in the poloidal direction. It was found that the direction of EC current reversed between ripple top heating and ripple bottom heating.

Acknowledgements

The authors would like to thank S. Kobayashi and S. Yamamoto for providing the data of the magnetic configurations of Heliotron J. This work is supported by Grant-in-Aid for Scientific Research (C) (20560764) and (S) (20226017) from JSPS, Japan.

[1] V. Ercmann and U. Gasparino, Plasma Phys. Control. Fusion **36**, 1869 (1994).
[2] R. Prater, Phys. Plasmas **11**, 2349 (2004).
[3] K. Nagasaki *et al.*, J. Plasma Fusion Res. **83**, 764 (2007).
[4] G. Motojima *et al.*, Nucl. Fusion **47**, 1045 (2007).
[5] K. Nagasaki *et al.*, Nucl. Fusion **50**, 025003 (2010).
[6] Y. Yoshimura *et al.*, Proceedings of ITC18 (2008) p.324.
[7] S. Murakami *et al.*, Nucl. Fusion **40**, 693 (2000).
[8] A. Boozer and G. Kuo-Petravic, Phys. Fluids **24**, 851 (1981).